IIETA International Information and Engineering Technology Association
Advancing the World of Information and Engineering

Mathematical Modelling of Engineering Problems
Vol. 9, No. 2, April, 2022, pp. 313-324
Journal homepage: http://iieta.org/journals/mmep

The Difference in the Wall Thickness of the Helicopter Structure Are Made of Composite Materials with Another Made of Steel

Emad Toma Karash[1*], Jamal Nayief Sultan[2], Majid Khaleel Najem[3]

[1] Mechanical Technology Department, Technical Institute, Northern Technical University, Mosul 41000, Iraq
[2] Power Mechanical Techniques Eng. Department, Tech. Engineering College, Northern Technical University, Mosul 41000, Iraq
[3] Technical Engineering College, Northern Technical University, Mosul 41000, Iraq

Corresponding Author Email: emadbane2007@ntu.edu.iq

https://doi.org/10.18280/mmep.090204

Received: 4 February 2022
Accepted: 6 April 2022

Keywords:
steel, helicopter, carbon fiber, fiber glass, composite materials, failure, structure

ABSTRACT

Weight is of great importance in the aircraft industry. Aircraft are made of aluminum alloys that are susceptible to heat treatment, because they are light in weight and are metal strong enough for the dynamic designed loads they can face, but there are other reasons for obtaining alternative materials, and these materials are composite materials that it is lighter in weight than aircraft made of aluminum, firstly, and secondly, it can be formed into attractive shapes, eliminating welding and rivets, and thirdly, it can be formed into aerodynamic shapes. This work is based on designing a three-dimensional model consisting of aluminum alloy (AA-6061-T6) of the structure helicopter and then comparing it with five other models of different metal and composite materials to obtain a structure that has the least weight among these models. The results indicate that the best model with the lowest weight is the fourth model consisting of carbon fiber, proportions and weight of a square meter and a thickness of (28 mm) than the weight of the first model consisting of aluminum and weighing (81 kg), it was less than (22.7%). Then the fifth model, which consisted of an outer layer of aluminum with a thickness of five millimeters and another inner layer of aluminum of the same thickness, and between the inner and outer layer eighteen layers of carbon fiber, where the percentage of decrease in it compared to the first model by up to (19.2%), and worse a model in terms of weight is the second model was made of steel, which has a weight that is almost twice the weight of the first model.

1. INTRODUCTION

Composite materials of laminated structure are extensively used in an aerospace application [1, 2]. They subjected to mechanical as well as to thermal loads which is caused by aerodynamic heating and severe thermal gradient built across the thickness of the material as a result a very high thermal stresses appeared, and the temperature increase affects the properties of material [1]. Laminated plate, and shells made of composite material was thermally stress analyzed. Finite element of semisoft shell and laminated plate was thermally stress analyzed. The results indicated that the laminates behavior in case of thermal load was different from that examined subjected to mechanical load [1]. Foreign objects impact on structures may produce an internal damage as a result strength of structure is occurs. Such impact study requires knowledge in event dynamic; predicating the induced damage extent, as well as structure residual properties needs to be estimated. The impact event involves the target motion, the projectile motion, and the local indentation on the contacted zone [2]. The traditional method to protect armored vehicles by armored based on steel could lead to a heavy structure which results a logistical problem appears due to the need of vehicles to transport to a battle site. Armored vehicle speed and mobility is of important needs in a combat situation, hence the decrease in the weight amount can lead to a faster vehicle speed and more maneuverable for a given power plant [3]. Fiber composite failure criteria thermal stresses effect was studied [4]. The study used a method of direct micromechanics for micro- thermal stress investigation effects on the composite failure envelope [4]. The exact failure envelope was developed by analyzing the composite by using FEA thermal stress. Affordable and Armored protection for combat vehicles was studied. Metallic advantages were described by different approaches. Various approach as well as advancement in the ceramic, metallic and armored of composite materials and armor system of new dynamic that are essentially adopted for survivability improvement of armored vehicles in the futuristic multispectral battlefield scenarios [5]. A helicopter windshield bird strike was investigated by applying finite element of smoothed particles hydrodynamic. Five cases were considered: acrylic of single layer, glass of single, acrylic of two walls, acrylic with polyvinyl butyral (PVB) interlayer and glass with PVB interlayer. It was concluded that windshield dramatically strength was increased by using PVB interlayer [6]. The performance of armored steel and its mechanical properties was studied, and the steel performance was determined by the material hardness, strength and its behavior to high strain. Adiabatic shear phenomenon, toughness, structural cracking was also studied along with its

specifications and standards. It was indicated that armored steel could improve the design well [7]. Rotary blades are an improvement in robotic design where fundamental aspects of aeronautical engineering (structure, performance and aerodynamics) are described and studied. A modular chassis and realistic composite rotor blades have been developed with advanced sectional commercial software architecture (VABS, ANSYS, Pre VABS) with a number of codes implemented to automate structural analysis ranging from aerodynamic data processing to stress analysis and sectional properties, a modular integration framework has been created in which Helicopter volume generation, structural analysis and aerodynamic performance analysis, as well as the manufacturing cost can be investigated. The movable part shall be aspects including the shape of the aileron, the internal structure and the shape of the plan considered in a multidisciplinary design improvement without an important exception to the configuration [8]. Rotorcraft structure structural in a multidisciplinary- environment was analyzed [9] and unconventional design concepts such as compound helicopters in which additional lifting surfaces as well as propellers were satisfied. Feature cut- out fusel lags of helicopter that influence the load path and hence the structure and mass. The process chain and the data format which was used to combine tools were described [9]. The main rotor craft design of new helicopters was the primary design objective for many years, and this design was developed and changed for the last couple of years into all helicopter components as an overall system assessment. The prediction of weight is an essential part of the design as it determines the rotorcraft basic properties. The rotor craft structure represents rotor craft major part; the structure air frame structural design constitutes a significant factor of the rotor craft at preliminary level [10]. Generally, the design of aircraft can be classified in to three classical as reported earlier [11]. The conceptual stage, the preliminary stage and the detailed design stage, weight assessment of rotorcraft structure in early design stages was investigated [12]. The rotorcraft design was carried out and also divided into three consecutive phases of: conceptual, preliminary as well as detailed design. The results of each phase have been served as input for the newly calculations which increased the detailed level and the new concept information. The rotorcraft weight drives the design of the propulsion system, rotors and the fuel required. Rotorcraft component weight estimation approach was shown by using statistical method which based on existing rotorcraft as well as using finite element methods approach which determined structural airframe weight based on mission profiles respectively bearable load cases [12]. Thermal deformation and stress in the slices were analyzed using equivalent single-layer models [13-18], There are variables that do not depend only on the number of layers, but on other variables, such as the armament directions of the layers, the impurities present between the layers and the very thin layers in which there is no armament between the layers, and the study of these variables can be observed in the works [19-22]. Composite materials have been used as materials in the manufacture of various material structures, as alternative materials to traditional materials, and good results have been obtained [23-25]. In addition, layer-wise models have been used to predict the thermal response of multilayer panels [26-28].

In this paper, Sex three-dimensional mathematical models will be created, consisting of different materials (aluminum, steel, fiber glass, carbon fiber, aluminum with carbon fiber, steel with carbon fiber). In order to obtain the best structure for a helicopter that is light in weight and that resists missiles under the influence of penetration pressure and high temperature, using the ANSYS 15.0 program.

2. MATERIALS AND MODEL ANALYSIS

Six three-dimensional models were created by fixing the width and height of the aircraft, where the largest dimensions were ($L = 15.56 * h = 5.23\ m$) respectively shown in Figure 1 and by changing the thickness of the helicopter structure to obtain the same specifications in the five models and take thickness of first model (Aluminum model ($t = 0.03\ m$)) in terms of its resistance to deformation and different stresses imposed on it, where a load of ($P = 500\ Pa$) with a temperature ($T = 250\ ^oC$) in a element on the structure of an area ($A_{element} = 0.30723\ m^2$) and as in Figure 1, using the ANSYS program (15.0).

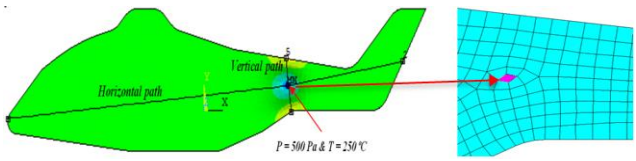

Figure 1. The geometry of the helicopter structure and the applied loads and the horizontal and vertical paths

Table 1 appears the mechanical and thermal specifications of the six models used in the tests in the ANSYS 15.0 program, the thickness of the wall of each model was chosen after simulation of attempts from taking different thickness for the five models and comparing the results of their resistance to deformation and different stress by providing an approach to the results of the tests of the first model, which consisted of aluminum alloy, in which the thickness of the model was fixed ($t = 0.03\ m$), and through repeated attempts the thickness and number of layers were determined for each model, while Table 2 shows the mechanical specifications of carbon fiber and fiberglass as orthotropic materials, as they have a modulus of elasticity, a modulus of stiffness and a different Poisson ratio in the three axes (x, y, z). As for the Table 3, it shows the type of model, the type of the applied load, and the type of the element used in the ANSYS 15.0 program, as well as the number of layers and their number in each model.

Table 1. Mechanical and thermal properties of aluminum alloy, steel, carbon fiber, and fiberglass [15-18, 24]

Model	*Materials*	*Density ρ, Kg/m³*	*Thermal Conductivity W/m.k*	*Melting Point, °C*	*Specific heat capacity, J/kg*	*Modulus of elasticity E, GPa*	*Passion's ratio*	*Number of layers*	*Total thickness t, (mm)*
M1	**Aluminum Alloy 6061 - T6**	2700	167	651	896	69	0.33	1	30
M2	**Steel**	7800	50.2	1540	470	210	0.3	1	20

M3	**Fiberglass**	**Glass 70%**	2500	0.8	1540	753	87	0.2	45	45
		Epoxy 30%	1200	0.23	84	1110	3.5	0.3		
M4	**Carbon fiber**	**Carbon 70%**	2267	0.17	3652	2020	230	0.3	28	28
		Epoxy 30%	1200	0.23	84	1110	3.5	0.3		
M5	**AA - 6061 - T6 & Carbon fiber**	**AA - 6061-T6**	2700	167	651	896	69	0.33	2	10
		Carbon 70%	2500	0.8	1540	2020	87	0.2	18	18
		Epoxy 30%	1200	0.23	84	1110	3.5	0.3		
M6	**Steel & Carbon fiber**	**Steel**	7800	50.2	1540	470	210	0.3	2	10
		Carbon 70%	2500	0.8	1540	2020	87	0.2	11	11
		Epoxy 30%	1200	0.23	84	1110	3.5	0.3		

Table 2. The flexible properties of fiberglass and carbon fiber [18]

Material	E_{ii}, MPa	G_{ii}, MPa	μ_{ij}	μ_{ji}
Carbon fiber	E_{11}=91600	G_{12}=11540	μ_{12}=0.26	μ_{21}=0.110
	E_{22}=38700	G_{13}=2750	μ_{13}=0.30	μ_{31}=0.028
	E_{33}=8590	G_{23}=1070	μ_{23}=0.30	μ_{32}=0.067
Fiberglass	E_{11}=26600	G_{12}=5030	μ_{12}=0.17	μ_{21}=0.150
	E_{22}=23300	G_{13}=1140	μ_{13}=0.52	μ_{31}=0.062
	E_{33}=10760	G_{23}=950	μ_{23}=0.53	μ_{32}=0.245

Table 3. The code, model, load type and element type used in the ANSYS 15.0 program

No.	Material	Code	Model	Individual disciplines	Type of Element
1	Model - 1	[0]	Linear, (Isotropic)	Structural & Thermal	SHELL 281
2	Model - 2	[0]	Linear, (Isotropic)		SHELL 281
3	Model - 4	[0/90/0/90/0/90/0/90/0/90/0/90/0/90/0/90/0/90/0/90/0/90/0/90/0/90/0/90/0/90/0/90/0/90/0/90]s	Linear (Orthotropic)		SHELL 281
4	Model - 3	[0/90/0/90/0/90/0/90/0/90/0/90/0/90/0/90/0/90/0/90/0/90/0/90/0/90/0/90/0/90/0/90/0/90/0/90]	Linear (Orthotropic)		SHELL 281
5	Model - 5	[0/0/90/0/90/0/90/0/90/0/90/0/90/0/90/0/90/0/90/0/90/0/90/0/90/0/90/0/90/0/90/0/90/0/90/0]	Linear, (Isotropic) Linear (Orthotropic)		SHELL 281
6	Model - 6	[0/0/90/0/90/0/90/0/90/0/90/0/90/0/90/0/90/0/90/0/90/0/90/0/90/0/90/0/90/0/90/0/90/0/90/0/90/0]	Linear, (Isotropic) Linear (Orthotropic)		SHELL 281

3. RESULTS AND DISCUSSION

The first model of aluminum alloy (AA-6061 T3) was designed in the ANSYS 15.0 program for a three-dimensional helicopter structure, as it was the maximum length (15.56 m) and the shortest width in the hull (5.23 m) while the wall thickness was (30 mm). The model was loaded with a pressure load (500 Pa) which is a temperature (250ºC) in the indicated area in the Figure 1 of the structure of the helicopter on an element whose cross-sectional area (0.30723), after calculating the maximum deformation and all the strains and stresses in the area of influence of the load, on a longitudinal and a transverse path, as indicated by the Figure 1. Five other models were then designed, made of different materials, some of which are composite materials, to compare their resistance to the same deformation, strains and stresses, and they have different wall thicknesses to obtain less weight for the structure of the helicopter, and it has the same specifications as the first model. Figure 2 shows a comparison between the maximum vectors deformations (U) in the different models and it is clear that the maximum deformation in the different models is almost equal despite the different materials used and the different wall thicknesses, the vectors deformations (U) value was confined between ($1.10*10^{-4}$ - $1.06*10^{-4}$).

The comparison of shear stress (σ_{xy}) results in Figure 3 for all models shows that the maximum stress was in the sixth model and its amount (6.50 MPa) while the lowest maximum stress was in the third model and its value was (1.82 MPa).

Figure 4 appears the results of comparing the stress intensity ($\sigma_{int.}$) for all models under the same loading conditions, and the figure shows that the maximum stress intensity was in the second model and its amount (42.1 MPa), and the lowest value of the stress intensity ($\sigma int.$) was in the third model and its value (7.57 MPa).

Figure 5 shows a comparison between the results of the strain ($\mathcal{E}_z$) of all the models, and shows that the results are in a very acceptable match, as the results of the strain were limited to ($1.03*10^{-4}$ - $3.13*10^{-4}$).

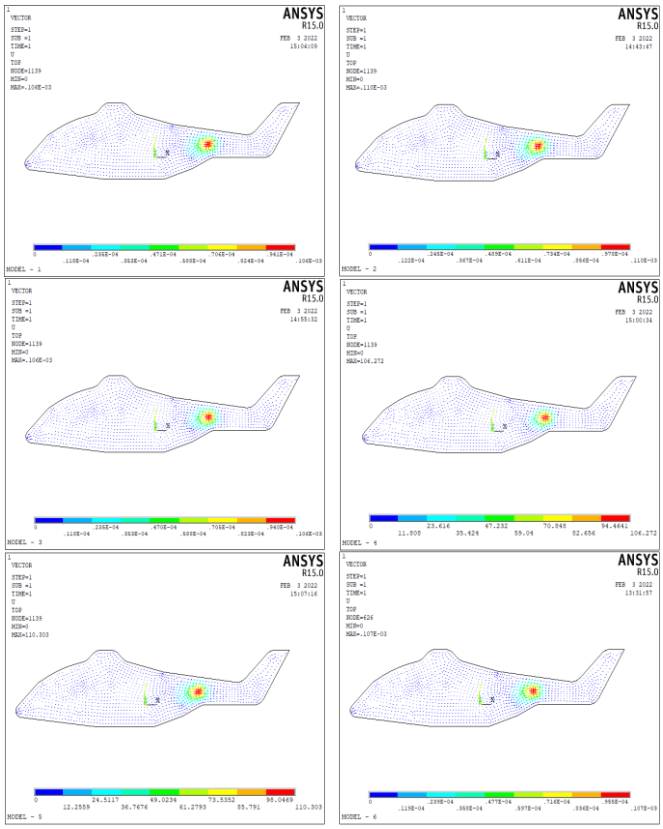

Figure 2. Results of vector deformation (U) for all models

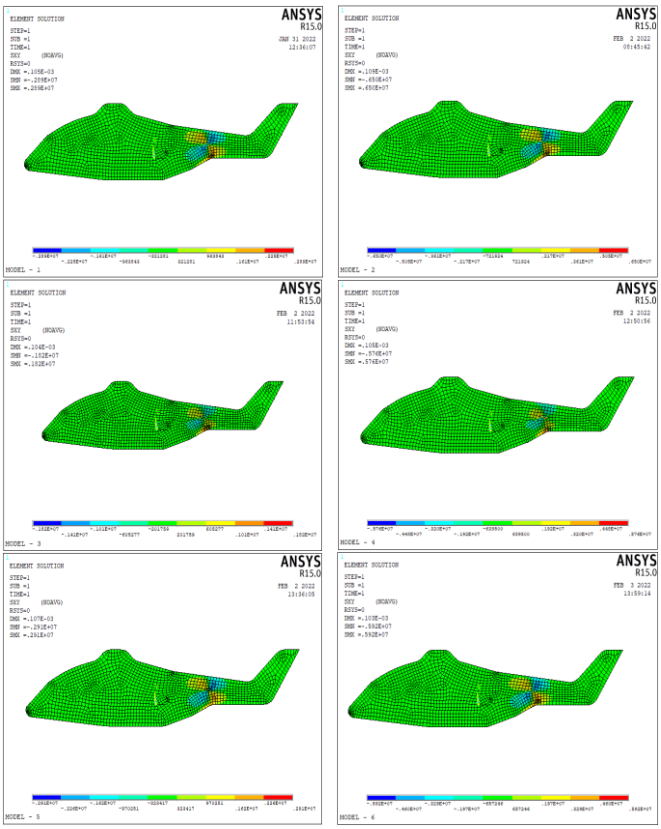

Figure 3. Results of normal shear stress (σ_{xy}) for all models

Figure 6 shows the results obtained for the different models of strain intensity ($\mathcal{E}_{int.}$), and the results were very close to each other and with a high degree of congruence, as the results were confined between ($2.39*10^{-4}$ - $5.93*10^{-4}$).

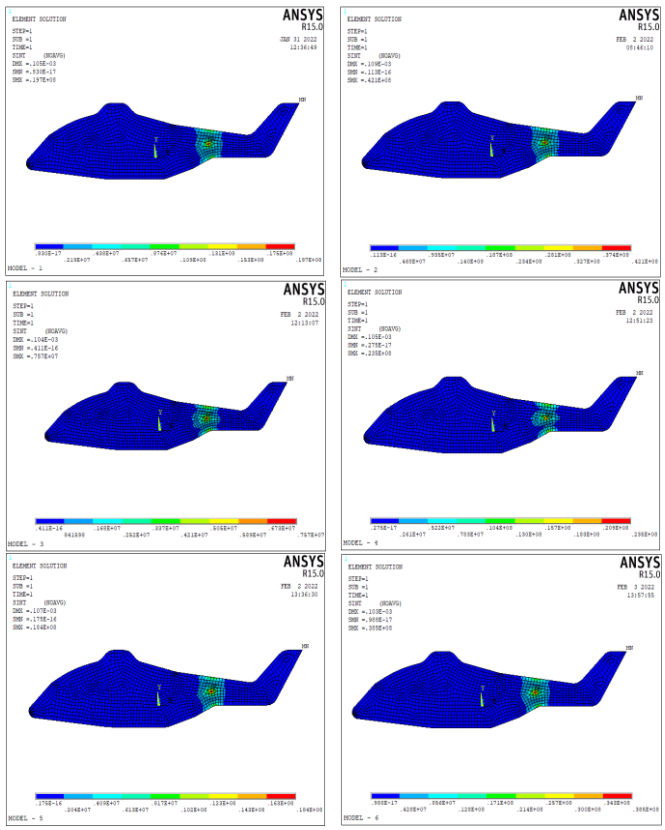

Figure 4. Results of Normal intensity r stress ($\sigma_{int.}$) for all models

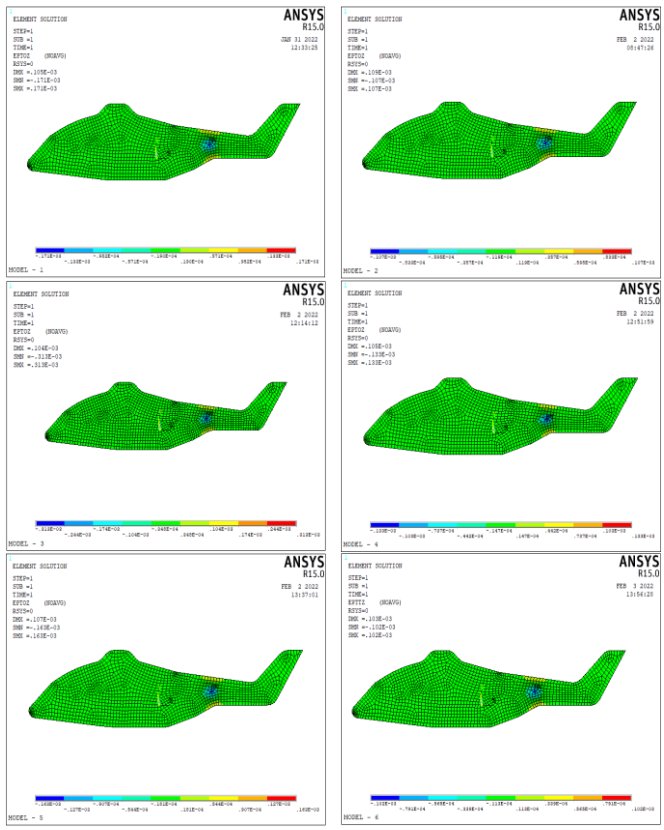

Figure 5. Results of total mechanical strain (ε_z) for all models

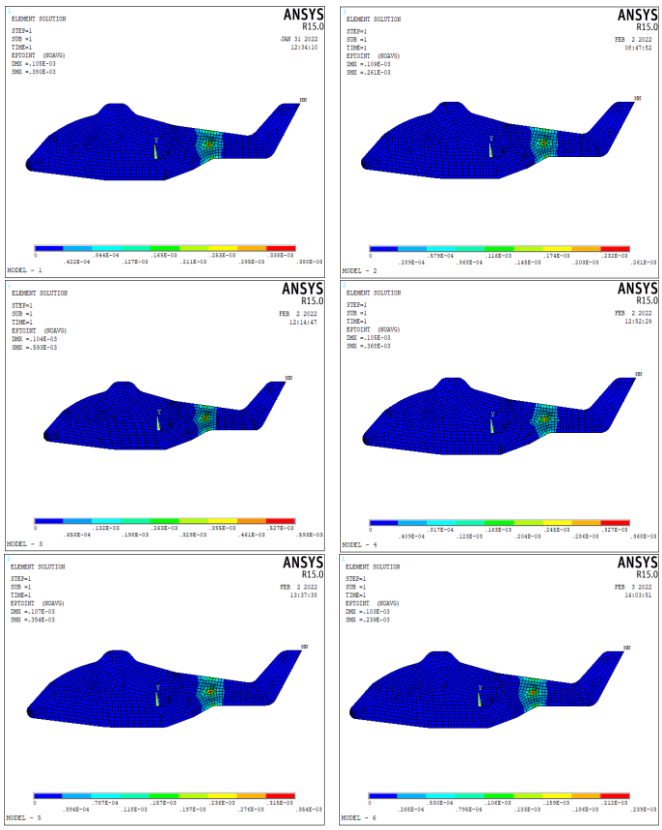

Figure 6. Results of total mechanical strain intensity ($\mathcal{E}_{int.}$) for all models

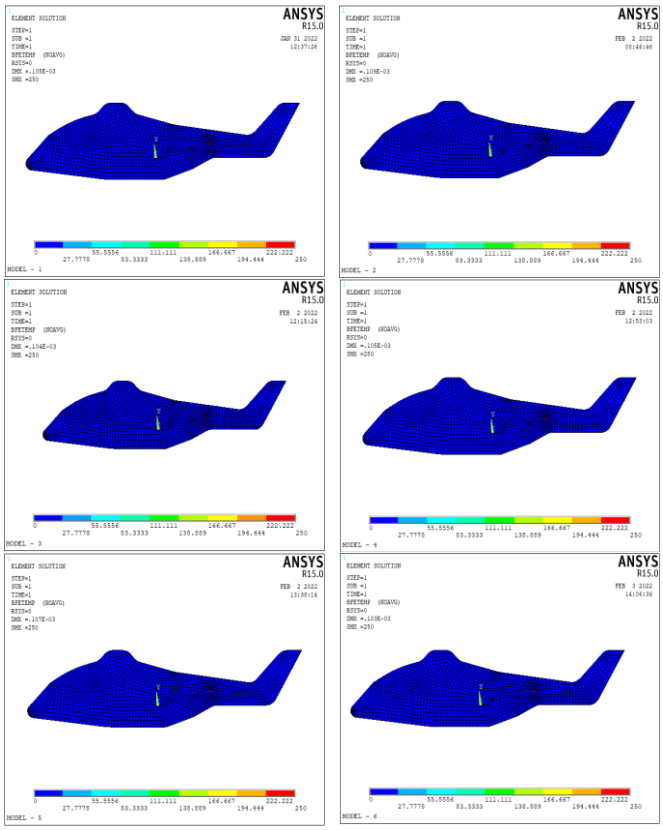

Figure 7. Results of body temperature (T_B) for all models

Figure 7 shows the effect of load temperature on the helicopter structure for all models, and the figures show that the temperature distribution is similar in almost all models.

Figure 8 shows the geometry deformation (*Uz*) along the horizontal path from the beginning to the end and passing through the region of influence of the loads, and it shows in the figure the maximum deformation in the region of the influence of the load, which has a similar shape in all models.

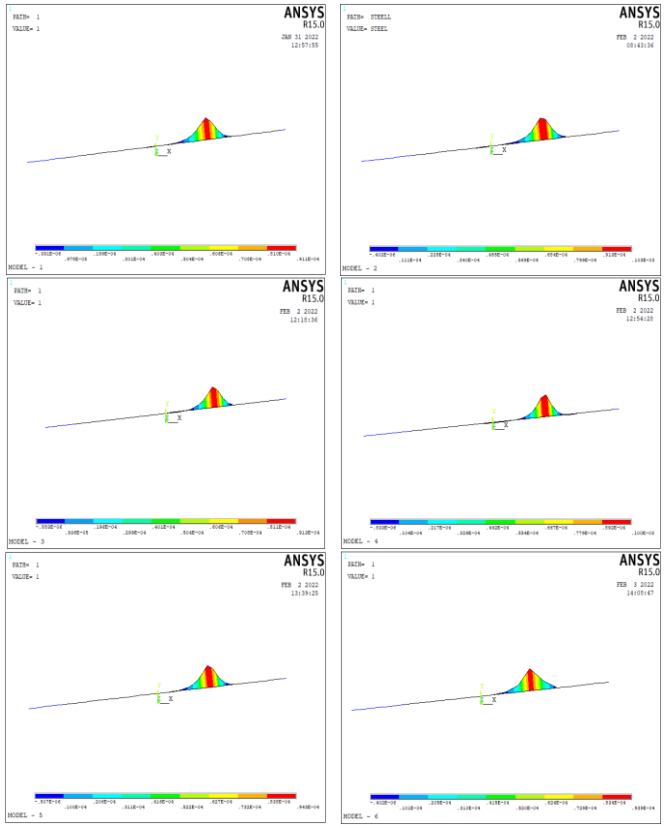

Figure 8. Results of geometry deformation (*Uz*) on horizontal path for all models

Figure 9 appears the comparison of the results of deformation in the direction of (*UZ*) on the vertical path, and from the figure shows a match in the resistance of the different models, which are of different thicknesses.

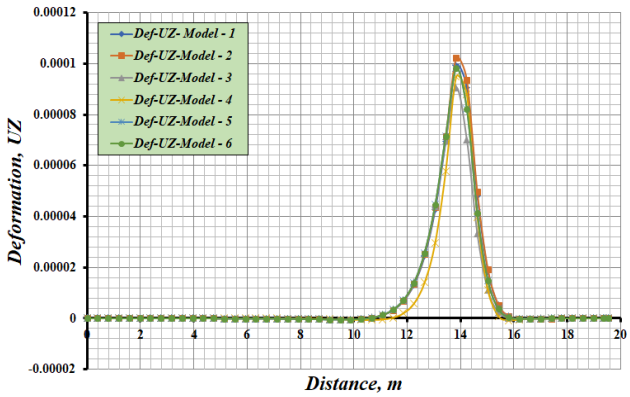

Figure 9. Comparison showing the result of deformation (*Uz*) on the horizontal path for all models

Figure 10 appears a comparison of the results obtained for axial deformation in the direction of (*ROTX*) on the vertical path, and from the figure it is clear that the maximum deformation value in the first model is less than that of the other models.

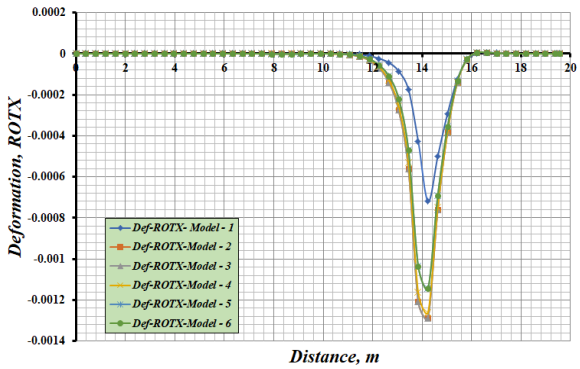

Figure 10. Comparison showing the result of deformation (*ROTX*) on the horizontal path for all models

Figure 11 appears a comparison of the results obtained for axial deformation in the direction of (*ROTY*) on the vertical path, and the figure shows that the maximum deformation value is identical in all models.

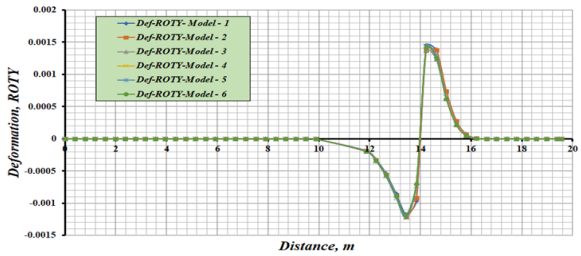

	Model - 1	Model - 2	Model - 3	Model - 4	Model - 5	Model - 6
Maximum Tension Deformation	0.00145	0.00139	0.00137	0.00130	0.00144	0.00142
At distance, m	14.23					
Maximum Compression Deformation	- 0.00117	- 0.00121	- 0.00118	- 0.00134	- 0.00122	- 0.00119
At distance, m	13.44					

Figure 11. Comparison showing the result of deformation (*ROTY*) on the horizontal path for all models

Figure 12 appears a comparison of the results obtained for axial deformation in the direction of (*ROTSUM*) on the horizontal path. The figure shows that the maximum deformation value was in the fifth model, and the deformation value was in the first mode, but the difference is very small between all models.

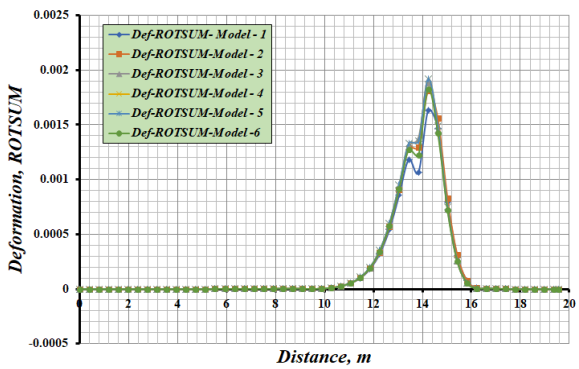

Figure 12. Comparison showing the result of deformation (*ROTSUM*) on the horizontal path for all models

Figure 13 appears a comparison of the results obtained for normal stress (σ_x) on the horizontal path. The figure shows that the maximum value of the stress was in the sixth model and then the fifth model, while the lowest value of the stress was in the third model, also the stress value in the first model was almost in the average stresses.

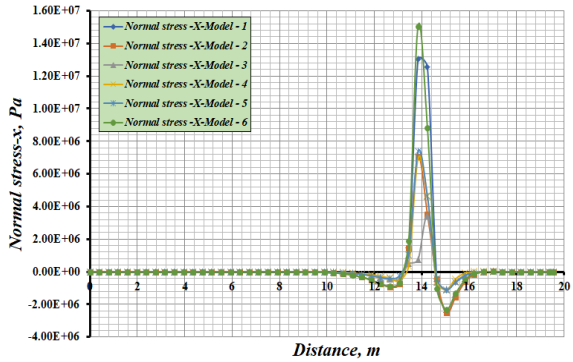

Figure 13. Comparison showing the result of normal stress (σ_x) on the horizontal path for all models

Figure 14 appears a comparison of the results obtained for normal stress (σ_y) results on the horizontal path, and that the maximum value of the stress was in the second model, while it was the lowest value of the stress in the third model, and the stress value in the first model was after the value of second model.

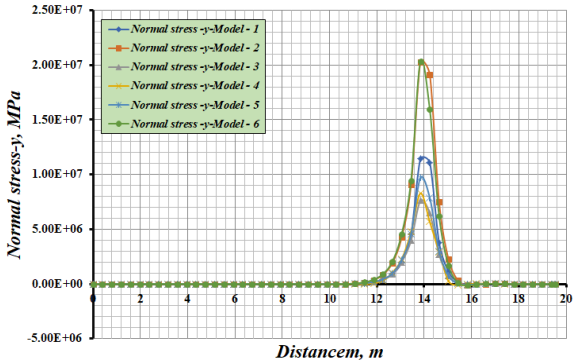

Figure 14. Comparison showing the result of normal stress (σ_y) on the horizontal path for all models

Figure 15 appears a comparison of the results obtained for shear stress (τ_{xy}) on the horizontal path, and that the maximum value of shear stress was in the second model when it was positive shear stress, while it was the lowest value of the negative shear stress in the sixth model, and the value of the other models was almost equal.

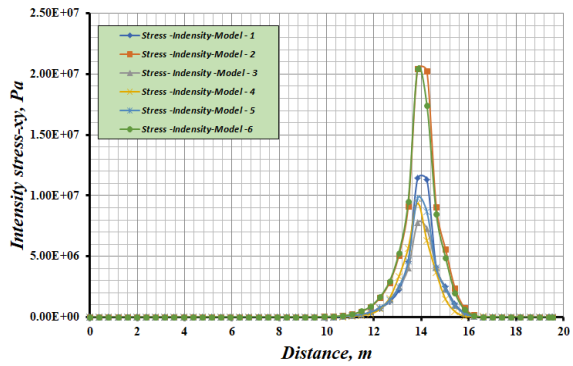

Figure 15. Comparison showing the result of shear stress (τ_{xy}) on the horizontal path for all models

Figure 16 appears a comparison of the results obtained for the stress intensity ($\sigma_{int.}$) on the horizontal path, and that the

maximum value of the stress intensity was in the second and sixth model, while it was the lowest value of the stress intensity in the third model, and the value of the other models was almost equal.

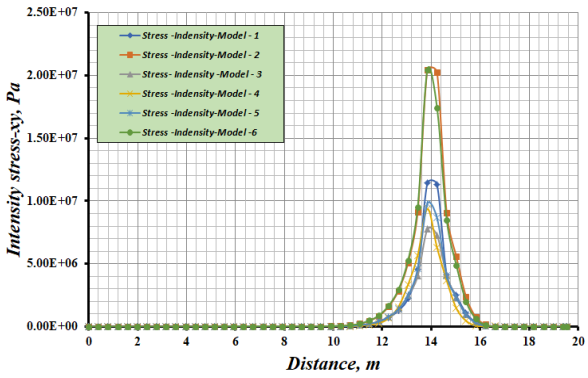

Figure 16. Comparison showing the result of intensity stress ($б_{int.}$) on the horizontal path for all models

Figure 17 appears a comparison of the results obtained of the stress results ($б_{von.}$) on the horizontal path, and that the maximum value of the stress intensity was in the second and sixth model, while the lowest value of the stress intensity was in the third model.

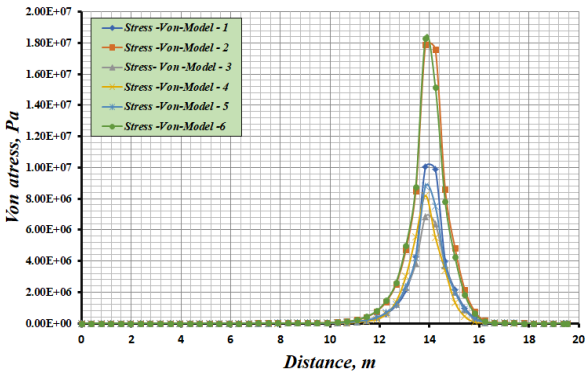

Figure 17. Comparison showing the result of intensity stress ($б_{von.}$) on the horizontal path for all models

Figure 18 shows the comparison of the results of the total strain-x ($\mathcal{E}_{x.}$) on the horizontal path, and an acceptable match is found in the results of all models.

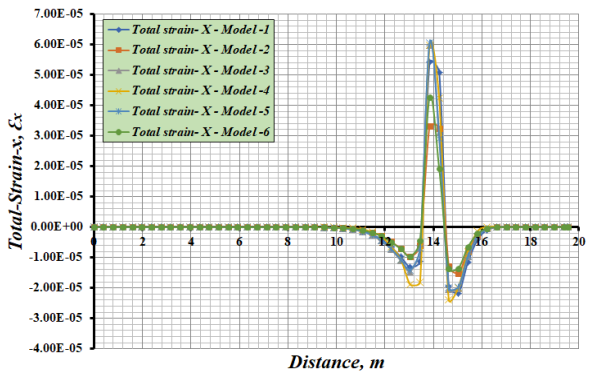

Figure 18. Comparison showing the result of total strain-x ($\mathcal{E}_{x.}$) on the horizontal path for all models

Figure 19 appears a comparison of the results obtained of the total strain ($\mathcal{E}_{y}$) on the horizontal path, and the highest strains are in the first models compared to the other models, it was the lowest value in the sixth model.

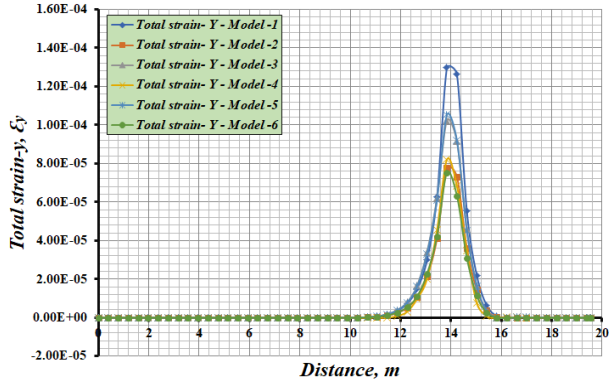

Figure 19. Comparison showing the result of total strain-y ($\mathcal{E}_{y.}$) on the horizontal path for all models

Figure 20 appears a comparison of the results obtained of the total strain ($\mathcal{E}_{z}$) on the horizontal path, and the highest strains are in the first and fifth models compared to the other models, whose values are to some extent identical.

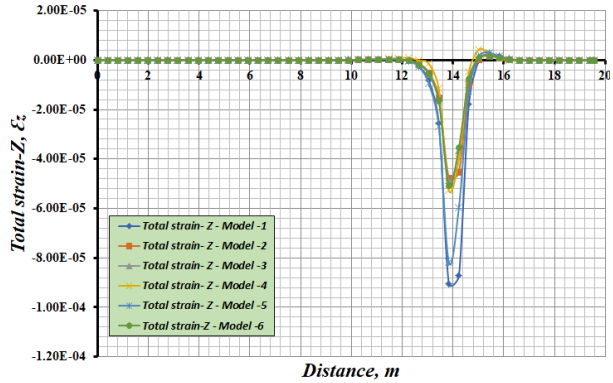

Figure 20. Comparison showing the result of total strain-z ($\mathcal{E}_{z}$) on the horizontal path for all models

Figure 21 appears a comparison of the results obtained of the results of the shear total strain ($\mathcal{E}_{xy}$) on the horizontal path, and the highest strains were in the fourth model compared to other models whose values were with an acceptable match.

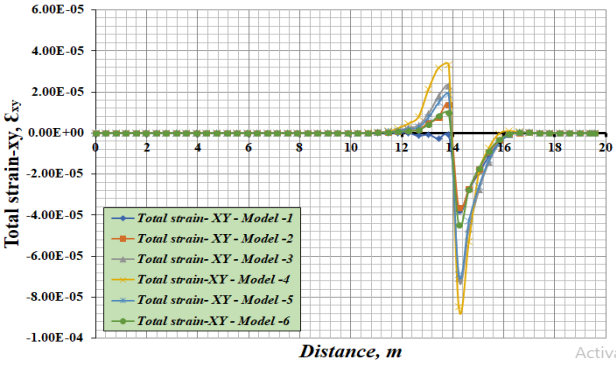

Figure 21. Comparison showing the result of total strain-xy ($\mathcal{E}_{x.y}$) on the horizontal path for all models

Figure 22 appears a comparison of the results obtained of the total strain intensity ($\mathcal{E}_{int.}$) on the horizontal path, and the values of the second and sixth was the lowest, while the models' values were variable in the region of the highest strain, and the highest value was in the first model.

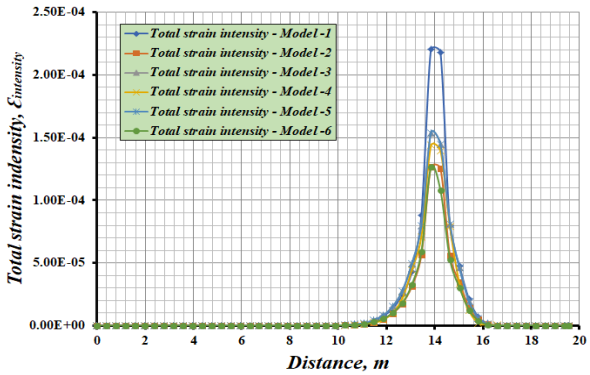

Figure 22. Comparison showing the result of total strain-intensity ($\mathcal{E}_{int.}$) on the horizontal path for all models

Figure 23 appears a comparison of the results obtained of the total von strain ($\mathcal{E}_{von}$) on the horizontal path, where the lowest values were in the second and fifth models, while the other model values were somewhat identical.

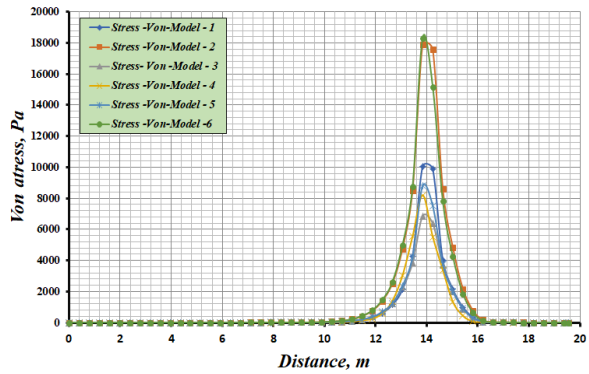

Figure 23. Comparison showing the result of total von strain ($\mathcal{E}_{von}$) on the horizontal path for all models

Figure 24 appears a comparison of the results obtained of the axial deformation in the direction of (*Uz*) on the vertical path, and it is clear from the figure that the maximum deformation value in all models is similar.

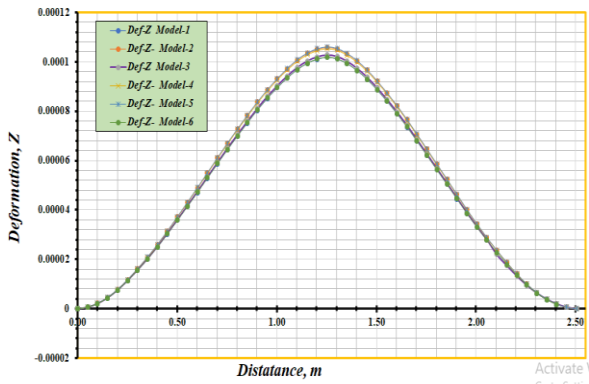

Figure 24. Comparison showing the result of deformation (*Uz*) on the vertical path for all models

Figure 25 appears a comparison of the results obtained of the axial deformation in the direction of (*ROTX*) on the vertical path, and it is clear from the figure that the maximum deformation value in all models is similar.

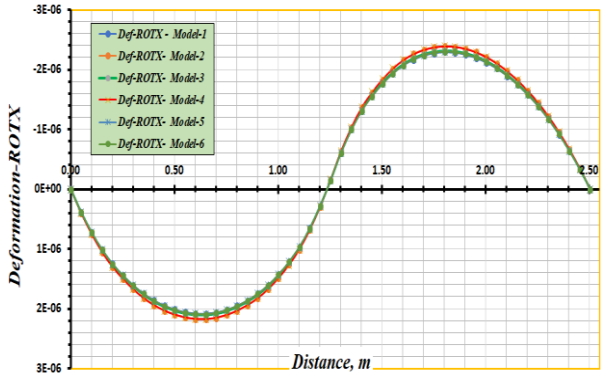

Figure 25. Comparison showing the result of deformation (*ROTX*) on the vertical path for all models

Figure 26 appears a comparison of the results obtained of the axial deformation in the direction of (*ROTY*) on the vertical path, and the figure shows that the maximum deformation value is identical in all models.

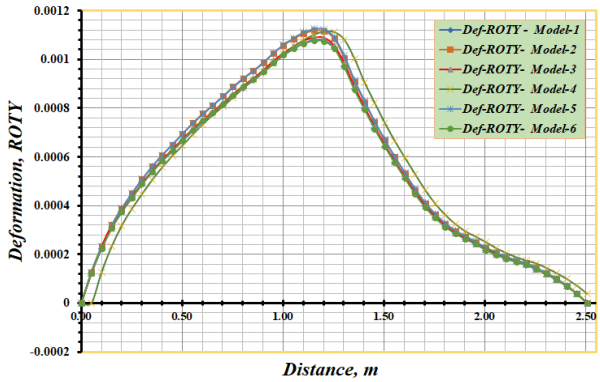

Figure 26. Comparison showing the result of deformation (*ROTY*) on the vertical path for all models

Figure 27 appears a comparison of the results obtained of the axial deformation in the direction of (*ROTSUM*) on the vertical path. The figure shows nearly identical deformation values in all six different models.

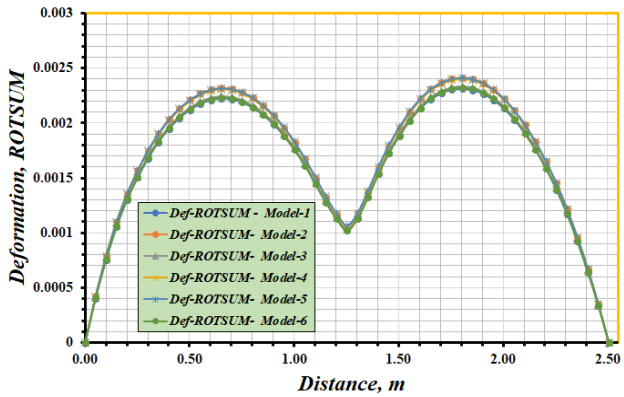

Figure 27. Comparison showing the result of deformation (*ROTSUM*) on the vertical path for all models

Figure 28 appears a comparison of the results obtained of the normal stress (σ_x) on the vertical path. The figure shows that the maximum value of the stress was in the second model, while the lowest value of the stress was in the third model.

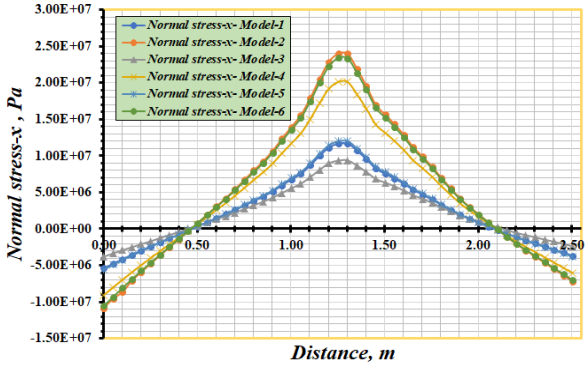

Figure 28. Comparison showing the result of normal stress (σ_x) on the vertical path for all models

Figure 29 appears a comparison of the results obtained of the normal stress (σ_y) results on the vertical path, and that the maximum value of the stress was in the second model, while it was the lowest value of the stress in the third model.

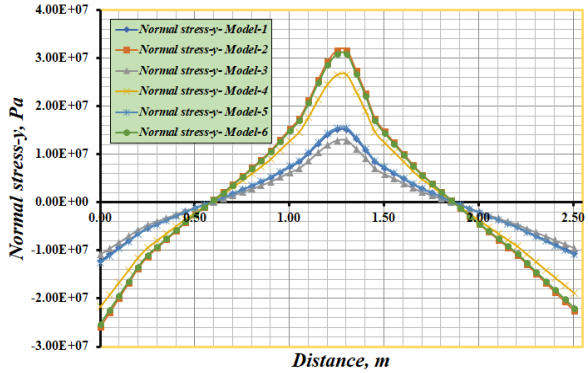

Figure 29. Comparison showing the result of normal stress (σ_y) on the vertical path for all models

Figure 30 appears a comparison of the results obtained of the shear stress results (τ_{xy}) on the vertical path, and that the maximum value of shear stress was in the second model when it was positive shear stress, while it was the lowest value of the negative shear stress in the first model, and the value of the other models was almost equal.

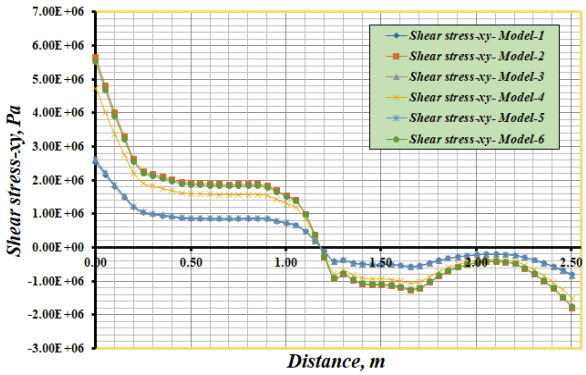

Figure 30. Comparison showing the result of normal stress (τ_{xy}) on the vertical path for all models

Figure 31 appears a comparison of the results obtained of the stress intensity ($\sigma_{int.}$) on the vertical path, and that the maximum value of the stress intensity was in the second and sixth model, while it was the lowest value of the stress intensity in the third model.

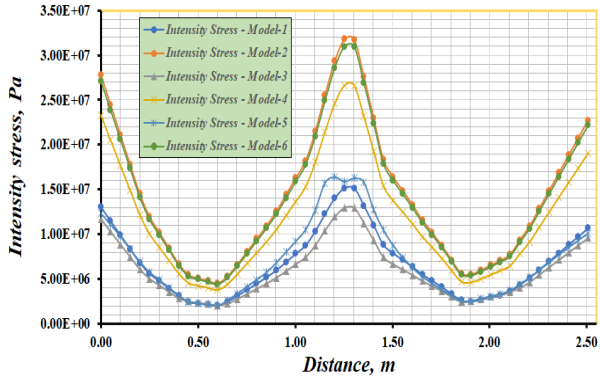

Figure 31. Comparison showing the result of intensity stress ($\sigma_{int.}$) on the vertical path for all models

Figure 32 appears a comparison of the results obtained of the von stress results ($\sigma_{von.}$) on the vertical path, and that the maximum value of the von stress was in the second model, while the lowest value of the stress intensity was in the third model.

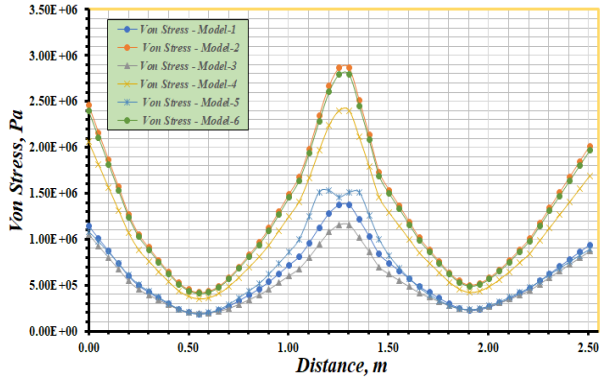

Figure 32. Comparison showing the result of intensity stress ($\sigma_{von.}$) on the vertical path for all models

Figure 33 appears a comparison of the results obtained of the total strain-x ($\mathcal{E}_x$) on the vertical path, and the strain was highest in the fourth model and lowest in the sixth model.

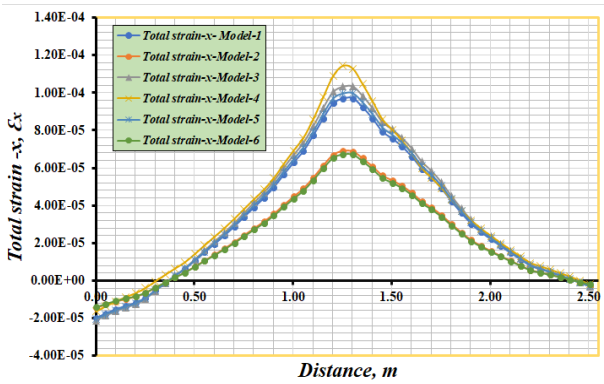

Figure 33. Comparison showing the result of total strain-x ($\mathcal{E}_{x.}$) on the vertical path for all models

Figure 34 appears a comparison of the results obtained of the total strain ($\mathcal{E}_y$) on the vertical path, and the highest strains are in the first models compared to the other models, it was the lowest value in the sixth model.

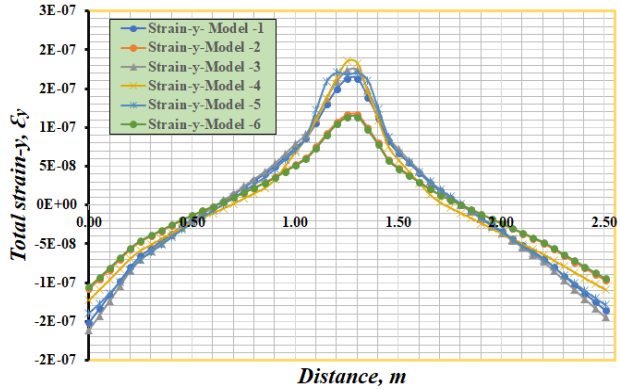

Figure 34. Comparison showing the result of total strain-y ($\mathcal{E}_{y.}$) on the vertical path for all models

Figure 35 appears a comparison of the results obtained of the total strain ($\mathcal{E}_z$) on the vertical path, and the highest strains are in the first and fifth models compared to the other models, whose values are to some extent identical.

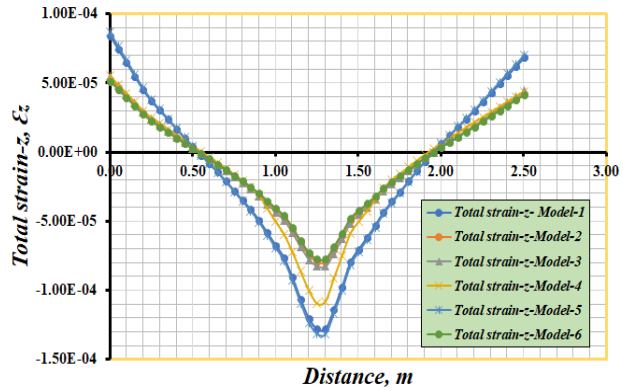

Figure 35. Comparison showing the result of total strain-z ($\mathcal{E}_z$) on the vertical path for all models

Figure 36 appears a comparison of the results obtained of the shear total strain ($\mathcal{E}_{xy}$) on the vertical path, and the highest strains were in the third model compared to other models whose values were with an acceptable match.

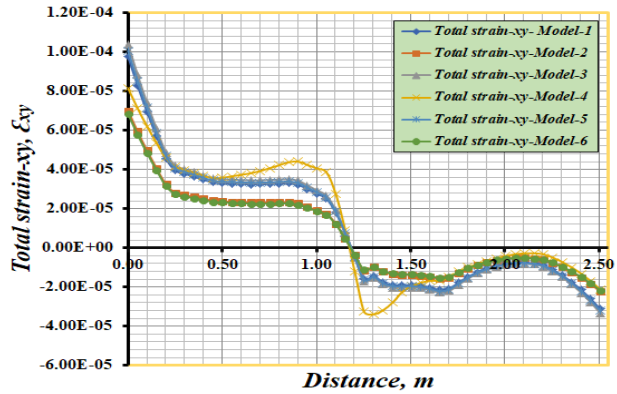

Figure 36. Comparison showing the result of total strain-xy ($\mathcal{E}_{xy}$) on the vertical path for all models

Figure 37 appears a comparison of the results obtained of the total strain intensity ($\delta_{int.}$) on the vertical path, and the value of the sixth was the lowest, and the highest value was in the second model.

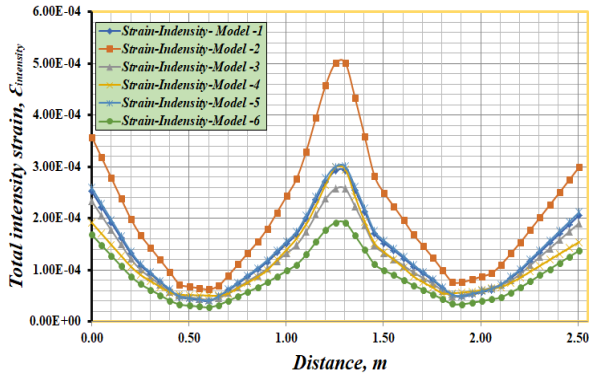

Figure 37. Comparison showing the result of total strain-intensity ($\mathcal{E}_{int.}$) on the vertical path for all models

Figure 38 appears a comparison of the results obtained of the total von strain ($\mathcal{E}_{von}$) on the vertical path, where the lowest values were in the second and sixth models, while largest value in the fourth model.

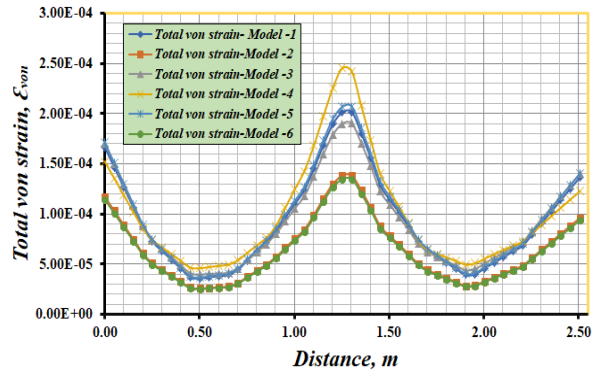

Figure 38. Comparison showing the result of total von strain ($\mathcal{E}_{von}$) on the vertical path for all models

Table 4 shows the results of all the tests for the six models that were designed in the ANSYS program to obtain better specifications for the wall of the structure of a helicopter.

The results in Table 4 show the following:

1. The weight of one square meter of the helicopter made of aluminum is (81 kg), as the lowest weight of the helicopter was when using carbon fiber materials, as the weight of one square meter was (54.51 kg) and thickness (28 mm), which is a decrease about aluminum by (22.7 %) and this is very better in terms of weight, followed by a wall consisting of an outer layer thick (5 mm) and an inner layer (5 mm) of aluminum and a middle layer of carbon fiber (18 mm thick), where the weight of the wall was per square meter (64 .98 mm), that is, less than a wall of aluminum by (19.2 %). It was higher and significantly higher than aluminum for a steel wall, where the weight was (156 kg) for one square meter of steel and (20 mm) thick, Where the percentage increase over the weight of aluminum by 93%.
2. The results indicate that the values of maximum deformation shape, total mechanical strain (ε_z) and

total mechanical strain intensity ($\varepsilon_{int.}$) are in an acceptable match.

3. The results in the above table indicate that the highest value of normal stress was in the sixth model (33 MPa), and the lowest value was in the third model (7.28 MPa), while the results of shear stress show that the highest value was in the fourth model (7.78 MPa) and the lowest in the third model (1.82 MPa). Also the results of stress intensity indicate that the highest value of the stress intensity was in the second model (42.57 MPa), while it was the lowest value in the third model (7.57 MPa), and these results of stresses show that the resistance of the third model is the weakest, While the optimum stress strength in the second model is very close to the values of the different stresses in the sixth model.

Table 4. The results of the six models tests using a ANSYS 15.0 program

Model	Materials	Density, ρ, Kg/m^3	*Deformation shape, Maximum*	*Normal stress stress-x, MPa*	*Shear stress stress-xy, MPa*	*Intensity stress, MPa*	*Total mechanical strain -z*	*Total mechanical strain intensity*	Number of layers	Total thickness, t, (*mm*)	Volume of wall, m^3	Weight, *of one square meter, (Kg)*	Percentage of the weight of a square meter of material compared to the weight of a square meter of aluminum %
M1	**Aluminum Alloy 6061 - T6**	2700	$1.05*10^{-4}$	16.1	2.85	19.7	$1.73*10^{-4}$	$3.8*10^{-4}$	1	30	0.03	81	---
M2	**Steel**	7800	$1.09*10^{-4}$	33	6.8	42.1	$1.07*10^{-4}$	$4.21*10^{-4}$	1	20	0.02	156	1.93
M3	**Fiberglass** **Glass 70%** **Epoxy 30%**	2500 1200	$1.04*10^{-4}$	7.28	1.82	7.57	$3.23*10^{-4}$	$7.57*10^{-4}$	45	45	0.045	94.95	1.17
M4	**Carbon fiber** **Carbon 70%** **Epoxy 30%**	2267 1200	$1.07*10^{-4}$	21	7.76	23.5	$1.33*10^{-4}$	$3.68*10^{-4}$	28	28	0.028	54.51	0.673
M5	**AA - 6061 - T6 & Carbon fiber** **AA - 6061** **Carbon 70%** **Epoxy 30%**	2700 2500 1200	$1.07*10^{-4}$	15.9	2.91	18.4	$1.63*10^{-4}$	$3.54*10^{-4}$	2 18	10 18	0.01 0.018	64.98	0.802
M6	**Steel & Carbon fiber** **Steel** **Carbon 70%** **Epoxy 30%**	7800 2500 1200	$1.04*10^{-4}$	33.3	6.02	39.4	$1.03*10^{-4}$	$2.43*10^{-4}$	2 11	10 11	0.01 0.011	101.21	1.25

4. CONCLUSIONS

The values of deformations, stresses, strains and temperature distribution were extracted in a three-dimensional model consisting of aluminum alloy (AA-6061- T6), and then five other models were designed with values of deformation resistance and resistance to stresses and strains close to the first model, but with different thicknesses to obtain the best structure with the least weight, The following conclusions were obtained:

1. The results show that the best weight obtained from a square of the structure of the helicopter was in the fourth model consisting of carbon fiber, where the weight was (54.41 kg) and the wall thickness was (28 mm), and then the fifth model, which consisted of aluminum alloy from the inside and outside with two layers, and between them carbon fiber with eighteen layers where the weight was (64.98 kg), but the worst model that had a large weight was the second model made of steel where the weight was (156 kg), despite the fact that its thickness was less compared to the other models, and the reason for this is its high density.
2. The values of resistance to deformations as shown by the figures in all results and in all directions (*UX, UY, UZ, ROTX, ROTY, ROTZ, ROTSUM*) were almost equal, meaning that the percentages of difference were very small.
3. There was a discrepancy in the values of all the different stresses (σ_x, σ_y, σ_z, τ_{xy}, τ_{yz}, τ_{xz}, $\sigma_{int.}$, σ_{von}) on the helicopter structure, in general, the maximum stresses were in the second model consisting of steel, and the lowest in the third model consisting of fiberglass, while the different stresses resistance values for the other models were between the values of the second and third models and the differences were between them in a rather small proportion.
4. The percentage of variance in the different strain resistance values (Ɛx, Ɛy, Ɛz, Ɛxy, Ɛyz, Ɛxz, Ɛint., Ɛvon) in all models was very small, and it can be said that the results, as shown in the figures for strain resistance, indicate that the strains are equal in all models.
5. The effect of high load temperature and its distribution on the surface of the helicopter's structure, as shown in the figures for the effect of temperature in the loading area on the helicopter's structure, was almost the same, as the difference ratios were very few in all models.

ACKNOWLEDGMENT

This research was supported by Engineering Science Research Program through the Northern Technical University / Technical Engineering college and Technical Institute of Mosul funded by the Ministry of Higher Education and Scientific Research / Republic of Iraq. (Grant No.: 00218-2021).

REFERENCES

[1] Thangaratnam, R.K., Ramachandran, J. (1988). Thermal stress analysis of laminated composite plates and shells. Computers & Structures, 30(6): 1403-1411. https://doi.org/10.1016/0045-7949(88)90204-0

[2] Abrate, S. (2001). Modeling of impacts on composite structures. Composite Structures, 51(2): 129-138. https://doi.org/10.1016/S0263-8223(00)00138-0

[3] Hogg, P.J. (2003). Composites for ballistic applications. Proceedings of Composite Processing, pp. 1-11. https://doi.org/10.1126/science.1131118

[4] Leong, M., Sankar, B.V. (2010). Effect of thermal stresses on the failure criteria of fiber composites. Mechanics of Advanced Materials and Structures, 17(7): 553-560. https://doi.org/10.1080/15376490903398706

[5] Vemuri, M., Bhat, B.T. (2011). Armour protection and affordable protection for futuristic combat vehicles. Defence Scientific Journal, 61: 394-402. https://doi.org/10.14429/dsj.61.365

[6] Hedayati, R., Ziaei-Rad, S., Eyvazian, A., Hamouda, A. M. (2014). Bird strike analysis on a typical helicopter windshield with different lay-ups. Journal of Mechanical Science and Technology, 28(4): 1381-1392. https://doi.org/10.1007/s12206-014-0125-3

[7] Cimpoeru, S.J. (2016). The mechanical metallurgy of armour steels. Defence Science and Technology Group Fishermans Bend VIC Australia. https://www.dst.defence.gov.au/sites/default/files/publications/documents/DST-Group-TR-3305_0.pdf.

[8] Vu, N.A., Lee, J.W., Le, T.P.N., Nguyen, S.T.T. (2016). A fully automated framework for helicopter rotor blades design and analysis including aerodynamics, structure, and manufacturing. Chinese Journal of Aeronautics, 29(6): 1602-1617. https://doi.org/10.1016/j.cja.2016.10.001

[9] Schwinn, D., Weiand, P., Schmid, M. (2017). Structural analysis of a rotorcraft fuselage in a multidisciplinary environment. In Summary of Proceedings. https://elib.dlr.de/112814.

[10] Schwinn, D.B., Weiand, P., Buchwald, M. (2020). Structural sizing of a rotorcraft fuselage using an integrated design approach. Journal of the American Helicopter Society, 65(4): 1-12. https://doi.org/10.4050/JAHS.65.042008

[11] Brown, C.D., Series, A.E. (1992). American Institute of Aeronautics and Astronautics, 370 L'Engant Promenade. SW, Washinton DC. https://arc.aiaa.org/doi/book/10.2514/4.104909

[12] Schwinn, D. B., Weiand, P., Buchwald, M. (2021). Rotorcraft fuselage mass assessment in early design stages. CEAS Aeronautical Journal, 12(2): 307-329. https://doi.org/10.1007/s13272-021-00492-z

[13] Reddy, J.N., Hsu, Y.S. (1980). Effects of shear deformation and anisotropy on the thermal bending of layered composite plates. Journal of Thermal Stresses, 3(4): 475-493. https://doi.org/10.1080/01495738008926984

[14] Khdeir, A.A., Reddy, J.N. (1991). Thermal stresses and deflections of cross-ply laminated plates using refined plate theories. Journal of Thermal Stresses, 14(4): 419-438. https://doi.org/10.1080/01495739108927077

[15] Kant, T., Khare, R.K. (1994). Finite element thermal stress analysis of composite laminates using a higher-order theory. Journal of Thermal Stresses, 17(2): 229-255. https://doi.org/10.1080/01495739408946257

[16] Robaldo, A. (2006). Finite element analysis of the influence of temperature profile on thermoelasticity of multilayered plates. Computers & Structures, 84(19-20): 1236-1246. https://doi.org/10.1016/j.compstruc.2006.01.022

[17] Cho, M., Oh, J. (2003). Higher order zig-zag plate theory under thermo-electric-mechanical loads combined. Composites Part B: Engineering, 34(1): 67-82. https://doi.org/10.1016/J.IJSOLSTR.2006.04.017

[18] Zhen, W., Wanji, C. (2009). A higher-order displacement model for stress concentration problems in general lamination configurations. Materials & Design, 30(5): 1458-1467. https://doi.org/10.1016/j.matdes.2008.08.013

[19] Sayyad, A.S., Ghugal, Y.M., Shinde, B.M. (2016). Thermal stress analysis of laminated composite plates using exponential shear deformation theory. International Journal of Automotive Composites, 2(1): 23-40. https://doi.org/10.1504/IJAUTOC.2016.078100

[20] Noor, A.K., Burton, W.S. (1992). Computational models for high-temperature multilayered composite plates and shells. Applied Mechanics Reviews, 45(10): 419-446. https://doi.org/10.1115/1.3119742

[21] Argyris, J., Tenek, L. (1997). Recent advances in computational thermostructural analysis of composite plates and shells with strong nonlinearities. Applied Mechanics Reviews, 50: 285-306. https://doi.org/10.1115/1.3101708

[22] Carrera, E. (2002). Temperature profile influence on layered plates response considering classical and advanced theories. AIAA Journal, 40(9): 1885-1896. https://doi.org/10.2514/2.1868

[23] Karash, E.T., Alsttar Sediqer, T.A., Elias Kassim, M.T. (2021). A comparison between a solid block made of concrete and others made of different composite materials. Revue des Composites et des Matériaux Avancés, 31(6): 341-347. https://doi.org/10.18280/RCMA.310605

[24] Najim, M., Sultan, J., Karash, E. (2020). Comparison of the resistance of soild shell of composite materials with other soild metal Materials. In: IMDC-SDSP 2020, pp. 28-30. https://doi.org/10.4108/eai.28-6-2020.2298518

[25] Karash, E.T. (2011). Modelling of unilateral contact of metal and fiberglass shells. In Applied Mechanics and Materials. 87: 206-208. https://doi.org/10.4028/www.scientific.net/AMM.87.206

[26] Cho, K.N., Striz, A.G., Bert, C.W. (1989). Thermal stress analysis of laminate using higher-order theory in each layer. Journal of Thermal Stresses, 12(3): 321-332. https://doi.org/10.2514/6.1989-1223

[27] Zhang, Z., Zhou, D., Fang, H., Zhang, J., Li, X. (2021). Analysis of layered rectangular plates under thermo-mechanical loads considering temperature-dependent material properties. Applied Mathematical Modelling, 92: 244-260. https://doi.org/10.1016/j.apm.2020.10.036

[28] Wu, Z., Chen, W, Ren, X. (2007). Refined global-local higher-order theory and finite element for laminated plates. International Journal for Numerical Methods in Engineering, 69(8): 1627-1670. https://doi.org/10.1016/j.compstruct.2008.06.011